Deformable Model-based PET Segmentation for Heterogeneous Tumor Volume Delineation

Mehrsima Abdoli, Rudi A. J. O. Dierckx and Habib Zaidi, *Senior Member, IEEE*

***Abstract*– PET-guided radiation therapy treatment planning, clinical diagnosis, assessment of tumor growth and therapy response are dependent on the accurate delineation of the tumor volume. Several PET segmentation techniques have been proposed in the recent years. Most these techniques fail in the presence of heterogeneity in the lesion. In this work, an active contour model based on the work presented by Chan and Vese (2001) is proposed to handle the heterogeneity of the lesion uptake. In the proposed method, the fitting terms in the Chan-Vese formulation are modified by introducing extra input images, including the smoothed version of the original image, using anisotropic diffusion filtering (ADF) and *à trous* wavelet transform of the image to handle the heterogeneity of the lesion uptake and avoid getting stuck in local minima. The advantage of utilizing ADF for image smoothing is that it avoids blurring the object's edges and preserves the average activity within a region, which is an important property for accurate PET quantification. The *à trous* wavelet transform is utilized due to its easy implementation and better performance at high noise levels. The algorithm was evaluated using seven clinical datasets with T3-T4 laryngeal squamous cell carcinoma from Louvain database where the 3D histology served as reference for comparison. Further evaluation was performed using phantom studies. The proposed method is also compared with a number of commonly used segmentation techniques, including fixed thresholding by 40% of the maximum SUV, the thresholding technique proposed by Nestle *et al*., and a fuzzy clustering-based approach (FCM). The quantitative data analysis shows that the segmented volumes using the proposed method have the highest overlap with the histology volumes. Moreover, the relative errors of calculated volumes and classification errors are lowest when using the proposed approach. Therefore, the proposed PET segmentation technique seems suitable for accurate tumor volume delineation.**

I. Introduction

PET-guided radiation therapy treatment planning, clinical diagnosis, assessment of tumor growth and therapy response are dependent on the accurate delineation of the tumor volume or gross tumor volume (GTV) for radiation therapy applications. However, the delineation of target volumes on PET images is known to be a challenging and complicated task due to the inherent noisy and low-resolution characteristic of PET images [1]. Manual delineation is vulnerable to intra- and inter-observer variability and is hardly reproducible. Therefore, automated segmentation techniques are the most appealing solutions to this problem, provided that they can achieve accurate and reliable results.

Several automatic and semi-automatic segmentation techniques have been proposed in the recent years with varying degrees of success. However, most of them fail in the presence of heterogeneity inside the lesion. In this work, an active contour model, based on the work presented by Chan and Vese [2] is proposed to handle the heterogeneity of the lesion uptake.

II. Materials and Methods

Active contour models attempt to deform and move an initial contour in a way that it matches the edges of the object. The classical active contour techniques construct a stopping edge-function based on the gradient of the image, in which the curve may get stuck in local minima states or pass through the object boundary since the discrete gradient is delimited and, as such, the stopping function might be never zero. In contrast, the Chan-Vese method [2] does not apply a stopping function and the stopping process is based on Mumford-Shah approach [3]. The energy functional used in Chan-Vese approach is as follows:

$$E(c_{in}, c_{out}, C) = \mu \,.\, Length(C) + \nu \,.\, Area(inside(C)) + \lambda_{in}\int_{inside(C)} \left|I(x,y) - c_{in}\right|^2 dx\, dy + \lambda_{out}\int_{outside(C)} \left|I(x,y) - c_{out}\right|^2 dx\, dy, \quad (1)$$

where C, the evolving curve in Ω, is defined as the boundary of an open subset ω of Ω, $I(x, y)$ is the gray scale image, C_{in} and C_{out} are the averages of $I(x, y)$ inside and outside C, respectively, and μ, ν, λ_{in} and λ_{out} are positive constants. The first two terms of the functional are regularizing terms and the last two terms are fitting terms.

A. Description of the proposed algorithm

In our proposed formulation, the fitting terms are modified by introducing extra input images to handle the heterogeneity of the lesion uptake and avoid getting stuck in local minima even further. The extra input images include the smoothed version of the original image, $I(x, y)$, using anisotropic

This work was supported by the Swiss National Science Foundation under grant SNSF 31003A-125246, Geneva Cancer League, the Indo-Swiss Joint Research Programme ISJRP 138866, and a research grant from Siemens Healthcare.

M. Abdoli is with Department of Nuclear Medicine and Molecular Imaging, University of Groningen, University Medical Center Groningen, Groningen, The Netherlands (e-mail: mehrsima.abdoli@gmail.com).

R. A. J. O. Dierckx is with Department of Nuclear Medicine and Molecular Imaging, University of Groningen, University Medical Center Groningen, Groningen, The Netherlands (e-mail: r.a.dierckx@umcg.nl).

H. Zaidi is with Division of Nuclear Medicine and Molecular Imaging, Geneva University Hospital, Geneva, Switzerland and Department of Nuclear Medicine and Molecular Imaging, University of Groningen, University Medical Center Groningen, Groningen, The Netherlands (e-mail: habib.zaidi@hcuge.ch)

diffusion filtering (ADF), and *à trous* wavelet transform of the image (Fig. 1). The advantage of utilizing ADF for image smoothing is that, in contrast to other smoothing filters, it avoids blurring of the object's edges. Moreover, using ADF preserves the average activity within a region, which is an important property for accurate quantification of PET data [4]. The ADF model is defined as follows:

$$\partial I_t^s = div\left(g\left(\left\|\nabla I^s\right\|\right)\nabla I^s\right), \qquad I^s(0) = I, \tag{2}$$

where I is the original gray scale image, I^s is the smoothed image, ∂I_t^s is the partial derivative of I with respect to diffusion time t, and g is the diffusivity function defined as

$$g(x) = \begin{cases} 1 & x \le 0 \\ 1 - exp\left(-3.15/(x/\eta)^4\right) & x > 0, \end{cases} \tag{3}$$

where η is the noise threshold estimated according to [5]. This function decreases rapidly for values higher than η which results in edge-preserving characteristic of ADF.

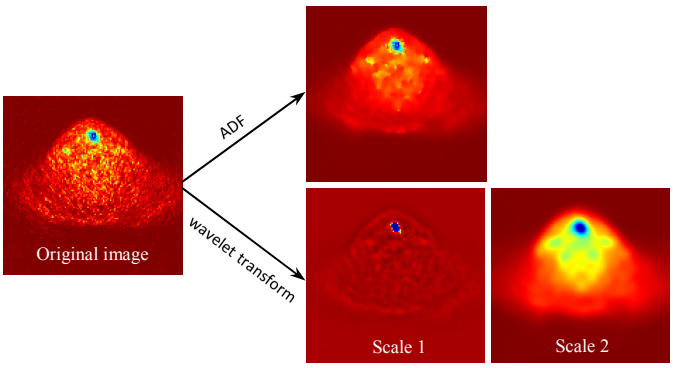

Fig. 1. Illustration of the proposed energy functional's input data.

The wavelet transform decomposes the original image into various wavelet scales, each of which represents specific features of the image. In our approach, the *à trous* wavelet transform [6] is applied due to its easy implementation and better performance at high noise levels. In the discrete wavelet transform, an analyzing wavelet is defined as $\Phi_{(s,l)}(x) = 2^{-s/2}\Phi\left(2^{-s}x - l\right)$, where s is the scale index and l is the location index. The scaling function Ψ of the analyzing wavelet Φ can be written as $\Psi(x) = \sum_{k=-1}^{N-2}(-1)^k c_{k+1}\Phi(2x+k)$, where c_k represents the wavelet coefficients. In *à trous* wavelet transform, the analyzing wavelet is defined as the difference between the scaling functions of two consecutive scales: $\frac{1}{2}\Phi\left(\frac{1}{2}\right) = \Psi(x) - \frac{1}{2}\Psi\left(\frac{x}{2}\right)$.

The correct scale has to be selected as the input to the energy functional to handle the heterogeneity of the lesion uptake. The first scale is not an appropriate choice since it mostly contains noise. The second and third scales are utilized in different circumstances. The second scale is used when the tumor-to-background ratio (TBR) and the lesion heterogeneity are low, and the third scale is used otherwise.

The energy functional used in this work can be written as follows:

$$E(c_{in}, c_{out}, C) =$$
$$\lambda_{in}\int_{in(C)}\left[\left|I(x,y) - c_{in}\right|^2 + \left|I^s(x,y) - c_{in}^s\right|^2 + \left|I^w(x,y) - c_{in}^w\right|^2\right]dx\,dy +$$
$$\lambda_{out}\int_{out(C)}\left[\left|I(x,y) - c_{out}\right|^2 + \left|I^s(x,y) - c_{out}^s\right|^2 + \left|I^w(x,y) - c_{out}^w\right|^2\right]dx\,dy, \tag{4}$$

where I^s is the smoothed image, c_{in}^s and c_{out}^s are the averages of I^s inside and outside the evolving contour C, respectively, I^w is the *à trous* wavelet transform of the original image I, c_{in}^w and c_{out}^w are the averages of I^w inside and outside the evolving contour, respectively. The regularizing terms used in Chan-Vese formulation are neglected since the second term has been set to zero by Chan and Vese and the first term does not effectively influence the curve evolution process in our experiments. The parameters λ_{in} and λ_{out} are determined by the user and depend on the lesion size, TBR and the lesion heterogeneity. In this work λ_{out} is set to 1 and only λ_{in} plays a role in the performance of the algorithm. Cases with large tumor size, high lesion heterogeneity and/or low TBR require higher value of λ_{in}.

Minimization of this energy functional is carried out using the level set formulation [7]. The level set method represents the evolving curve by the zero level set of a Lipschitz function $\phi : \Omega \to \mathbb{R}$, such that the value of the function ϕ is positive inside C and negative outside. In the energy formulation the variable C is replaced by ϕ and the energy functional is minimized with respect to ϕ using the Euler-Lagrange equation.

B. Phantom and clinical studies

The algorithm was evaluated using two separate phantom studies. The 4D extended cardio-torso (XCAT) phantom [9] is the first phantom used for evaluation. To simulate an irregular shaped tumor with heterogeneous uptake, we followed the procedure proposed by Le Maitre *et al* [10], except for the data simulation step where we applied an analytical simulator incorporated in the Software for Tomographic Image Reconstruction (STIR) package [11].

The second data sets are taken from the Zeolite phantom, in which samples of clinoptilolite (a family of natural zeolites), with ability of absorbing aqueous solutions of ^{18}F-FDG, are used to simulate irregularly shaped lesions [12].

Further evaluation of the technique was performed using seven clinical datasets with T3-T4 laryngeal squamous cell carcinoma from Louvain database [8]. The 3D volume of the lesions obtained from the surgical specimen is used as reference for evaluation.

The proposed method is also compared with a number of commonly used segmentation techniques, including thresholding by 40% of the maximum SUV (SUV_{max40}), a

thresholding technique proposed by Nestle *et al*. where the threshold is calculated based on the mean intensity within the tumor and the background [13], and a fuzzy clustering-based approach (FCM) [14].

C. *Evaluation metrics*

The evaluation metrics used for evaluation of the segmentation accuracy are as follows: (i) Mean relative error, which compares the volumes, (ii) spatial overlap index (SOI), which is defined in terms of pixel ratio of the overlapping regions A and B:

$$\mathrm{SOI} = \frac{2(\mathrm{A} \cap \mathrm{B})}{(\mathrm{A} + \mathrm{B})}$$

And (iii) classification error (*CE*) calculated voxel-by-voxel based on the following formula:

$$CE = \frac{(PCE + NCE)}{VoIL} \times 100\%$$

where *PCE* is the positive classification error and *NCE* is the negative classification error, and *VoIL* is the actual number of voxels reflecting the ground truth.

III. Results

The proposed segmentation technique was applied to the XCAT phantom and the obtained contour was compared to the ones obtained by the other segmentation techniques introduced in section II.B (Fig. 2). The simulated irregular shaped tumor with heterogeneous uptake is presented separately in Fig. 2a in three different views. Fig. 2b represents the segmentation results obtained by the proposed technique as well as three other common methods.

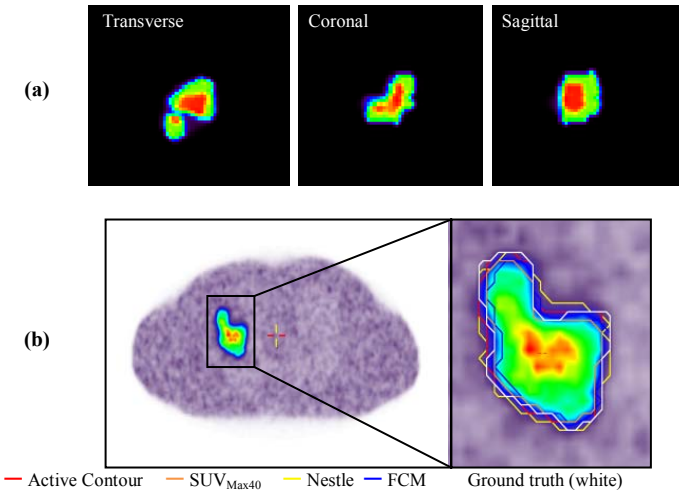

Fig. 2. (a) The realistic irregularly shaped simulated lesion defined on XCAT phantom with heterogeneous uptake. (b) Segmentation of the simulated tumor using the proposed method and three other segmentation techniques and comparison by the true volume.

Since the true volume of the simulated lesion is known, the accurate quantitative analysis of the data is performed in the same manner as the clinical studies. Table I summarizes the quantitative analysis for this phantom study.

TABLE I. QUANTITATIVE ANALYSIS OF SEGMENTATION RESULTS OF THE REALISTIC TUMOR SIMULATED ON THE XCAT PHANTOM OBTAINED BY THE PROPOSED AND OTHER SEGMENTATION TECHNIQUES.

Segmentation method	Mean volume (cc)	SOI	Relative error (%)	Classification error (%)
SUV_{max40}	22.52	0.75	24.44	24.81
Nestle	35.51	0.80	19.11	24.63
FCM	23.45	0.76	21.33	23.70
Active contour	30.87	0.88	3.56	12.49
True volume	29.81	-	-	-

The proposed technique was also validated using a second phantom study in which an experimental Zeolite phantom is used. In this phantom, 11 lesions are considered and the known true volumes of the lesions serve as ground truth for assessment. Fig. 3 illustrates a representative image of the phantom and the results obtained by different segmentation techniques. The quantitative analysis of the data is presented in table II.

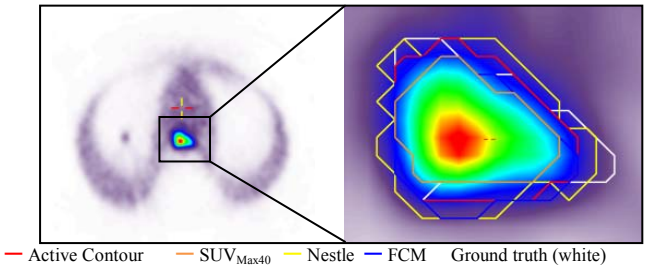

Fig. 3. Representative Zeolite phantom image and comparison of the results obtained by the proposed method and three other segmentation techniques.

TABLE II. QUANTITATIVE ANALYSIS OF THE ZEOLITE PHANTOM RESULTS OBTAINED USING THE PROPOSED AND OTHER SEGMENTATION TECHNIQUES.

Method	Mean volume (cc)	SOI	Relative error (%)	Classification error (%)
SUV_{max40}	1.39±0.61	0.50±0.08	49.15±9.23	50.18±7.94
Nestle	3.41±1.47	0.64±0.06	26.96±18.10	46.21±6.04
FCM	2.14±1.22	0.55±0.15	23.31±19.95	49.31±12.90
Active Contour	2.24±1.39	0.65±0.16	20.71±24.45	37.94±14.45
True Volume	2.71±1.24	-	-	-

Fig. 4 presents a representative example showing a comparison of the proposed segmentation technique with the contour obtained from the surgical specimen (Fig. 4b). The results of other segmentation approaches are also compared to the histology contour in Fig. 4c.

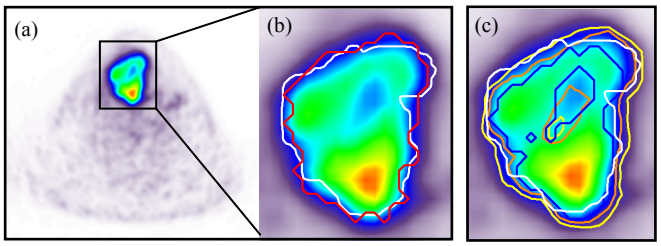

Fig. 4. Representative clinical PET image (a). Comparison of the result obtained by the proposed method and the histology (b). Comparison of three other segmentation techniques and the histology (c).

It can be observed that the proposed active contour model outperforms other segmentation techniques in terms of handling the lesion heterogeneity. The quantitative analysis of the data using the metrics introduced in section II.C is summarized in table III.

TABLE III. QUANTITATIVE ANALYSIS OF THE CLINICAL RESULTS OBTAINED USING THE PROPOSED AND OTHER SEGMENTATION TECHNIQUES.

Method	Mean volume (cc)	SOI	Relative error (%)	Classification error (%)
SUV_{max40}	31.49±11.90	0.40±0.20	208.13±225.12	226.82±213.53
Nestle	31.87±13.68	0.39±0.17	177.81±142.01	191.34±139.48
FCM	15.85±7.11	0.50±0.08	35.58±65.33	83.10±42.05
Active Contour	16.09±9.43	0.57±0.12	19.51±51.23	52.70±15.11
Histology	15.15±10.96	-	-	-

IV. DISCUSSION

The proposed deformable active contour model can be used to delineate heterogeneous tumor volumes on PET images. Application of ADF filter, with the capability of preserving the object's edges and also the mean intensity inside the object, makes it possible to handle the high level of noise in PET images in an appropriate manner, without influencing the quantification of the PET data. Moreover, the high performance of the *à trous* wavelet transform in the presence of high levels of noise makes it a suitable choice for handling the heterogeneity of the tumor. The original PET image is still being used as an input to the proposed energy functional since the second and third inputs suffer from higher partial volume effects compared to the original image, although the selected techniques to obtain the smoothed and the wavelet transform of the image are those that make this effect minimized.

The correct setting of the parameters λ_{in} and λ_{out} can greatly influence the final segmentation result, which makes the proposed method to be susceptible to fail when the parameters are not chosen carefully. To minimize this flaw we set one parameter (λ_{out}) to 1 throughout the experiments so that only one parameter needs to be determined by the user. According to the experiments we have carried out, determination of this parameter is highly dependent on the lesion size, TBR and the level of lesion heterogeneity. For larger tumor sizes, lower TBR and/or higher lesion heterogeneity require higher value of this parameter. Nevertheless, a clear and precise consensus of the choice of the parameter needs to be made to make the segmentation technique more robust.

V. CONCLUSION

In this study, a deformable active contour model is proposed to delineate heterogeneous tumors on PET images. The quantitative analysis of the segmentation results using the three evaluation metrics (mean relative error, SOI and classification error) reveals that the segmented volumes using the proposed method have the highest overlap with the histology volumes and the true volume of the phantom tumors. Moreover, the relative and classification errors are the lowest when the proposed approach is utilized. Therefore, the use of the proposed segmentation technique results in more accurate tumor volume delineation.

ACKNOWLEDGEMENTS

This work was supported by the Swiss National Science Foundation under grant SNSF 31003A-125246, Geneva Cancer League, the Indo-Swiss Joint Research Programme ISJRP 138866, and a research grant from Siemens Healthcare. The authors are indebted to AAPM Task group TG211 for providing the clinical and experimental phantom studies used in this work.

REFERENCES

[1] H. Zaidi and I. El Naqa, "PET-guided delineation of radiation therapy treatment volumes: a survey of image segmentation techniques," *Eur J Nucl Med Mol Imaging,* vol. 37, pp. 2165-87, Nov 2010.

[2] T. F. Chan and L. A. Vese, "Active contours without edges," *IEEE Trans Image Process,* vol. 10, pp. 266-277, 2001.

[3] D. Mumford and J. Shah, "Optimal approximations by piecewise smooth functions and associated variational problems," *Communications on Pure and Applied Mathematics,* vol. 42, pp. 577-685, 1989.

[4] J. Weickert, *Anisotropic diffusion in image processing*. Stuttgart, Germany: B. G. Teubner Stuttgart, 1998.

[5] J. Canny, "A Computational Approach to Edge-Detection," *Ieee Transactions on Pattern Analysis and Machine Intelligence,* vol. 8, pp. 679-698, 1986.

[6] J. L. Strack, F. Murtagh, and A. Bijaoui, *Image processing and data analysis*. Cambridge: Cambridge University Press, 1998.

[7] S. Osher and J. A. Sethian, "Fronts Propagating with Curvature-Dependent Speed - Algorithms Based on Hamilton-Jacobi Formulations," *Journal of Computational Physics,* vol. 79, pp. 12-49, 1988.

[8] X. Geets, J. A. Lee, A. Bol, M. Lonneux, V. Gregoire, "A gradient-based method for segmenting FDG-PET images: methodology and validation," *Eur J Nucl Med Mol Imaging,* vol. 34, pp. 1427-38, 2007.

[9] W. P. Segars, G. Sturgeon, S. Mendonca, J. Grimes, B. M. Tsui, "4D XCAT phantom for multimodality imaging research," Med Phys, vol. 37(9), pp. 4902-15, 2010.

[10] A. Le Maitre et al, "Incorporating Patient-Specific Variability in the Simulation of Realistic Whole-Body ^{18}F-FDG Distributions for Oncology Applications," *Proceedings of the IEEE*, vol. 97(12), pp. 2026-38, 2009.

[11] K. Thielemans et al, "STIR: Software for Tomographic Image Reconstruction Release 2," *Phys Med Biol*, vol. 57(4), pp. 867-83, 2012.

[12] F. Zito et al, "The use of zeolites to generate PET phantoms for the validation of quantification strategies in oncology," *Med Phys*, vol. 39(9), pp. 5353-61, 2012.

[13] U. Nestle et al, "Comparison of different methods for delineation of 18F-FDG PET-positive tissue for target volume definition in radiotherapy of patients with non-Small cell lung cancer," *J Nucl Med,* vol. 46, pp. 1342-8, 2005.
[14] J. Bezdek, R. Hathaway, M. Sabin, and W. Tucker, "Convergence theory for fuzzy c-means: counterexamples and repairs," *IEEE Trans Syst Man Cybern*, vol. 17, pp. 873-877, 1987.